Journal of Microelectronics and Electronic Packaging (2008) **5**, 142-149

ISSN: 1551-4897

Systematic Characterization of Embossing Processes for LTCC Tapes

Heike Bartsch de Torres,* Robert Gade, Arne Albrecht, and Martin Hoffmann

Abstract—**Embossing of LTCC green tapes allows the defined patterning of conductor paths and fluidic channels with excellent edge molding. However, basic process settings have not systematically been investigated up to now. We present a comprehensive overview, regarding basic process variables and new manufacturing approaches. Because the molding quality depends on the viscoelastic properties of the tape, rheological measurements were carried out. The influence of the basic process parameters, that is, temperature, pressure, time, and friction, were investigated systematically under the use of design of experiments. The influence of these parameters on the forming of micropatterns down to 10 μm was investigated, as also were the stress of the tape caused by the plastic deformation, the accuracy of edge molding, and the demolding behavior of the embossed tape. Optimum parameters were derived. From the analysis of variances it is clear that friction exerts the most important influence on the molding of fine patterns. Position tolerances of embossed patterns were determined and relaxation effects studied in order to ensure stable process conditions. It was possible to improve the leakage characteristics of valve seats by making use of embossed patterns such as smoothed metallization and a three-dimensional sealing ring. The leakage characteristic of valve seats could be improved by a factor of four.**

Keywords—**LTCC, viscoelastic properties, embossing, design of experiments, micro valves, sealing**

Introduction

Low temperature cofired ceramics (LTCC) are promising multipurpose materials in the focus of the present-day MEMS research. They combine electronic functionality and easy generation of three-dimensional geometry and thereby enable smart sensor solutions [1]. Their excellent chemical resistance and heat stability makes them stand out for use in microfluidic systems [2]. The whole range of cost-effective thick film technologies is available for use in the materials systems covered in this work. Supplementary techniques such as embossing or acetone jet etching [3] complete the manufacturing scope. In recent years, embossing has been the focus of several investigations under different application aspects. In combination with the LTCC-M technology, vacuum-tight barriers were embossed in LTCC and used to fabricate PDP back panels with HDTV resolution [4]. It was shown that filling of embossed patterns with conductor pastes will produce high-ampacity coils [5]. Even large cavities can be embossed into ceramic multilayers [6, 7]. A successful combination of hot embossing with a zero-shrinkage sintering technique has been demonstrated [8]. The possibility of forming fine fluidic channels without any additives has been explored [9]. Further development toward complex fluidic systems requires regulating units such as fully integrated valves. The challenge within the manufacturing of such elements is the generation of functional patterns that allow adequate sealing despite the limited forces, strength, and accuracy that go along with thick film technologies. One approach to meeting these demands is the generation of precise micropatterns by means of embossing. Therefore it is necessary to get a better comprehension of the embossing process. With this goal, the basic parameter field is characterized systematically. For this purpose, the investigation of the viscoelastic tape character is a first step in understanding the forming process.

Manuscript received August 2008 and accepted February 2009
TU Ilmenau, Institute for Micro- and Nanotechnologies, G.-Kirchhoff-Str. 7, 98693 Ilmenau, Germany
*Corresponding author; email: Heike.Bartsch@TU-Ilmenau.de

Viscoelastic Properties of LTCC Tape

A. Applied Rheological Principles

LTCC green tapes are filled polymers with a filler concentration usually above 60%. The Burgers model, a combination of a Maxwell and a Kelvin-Voigt element, describes their rheological behavior. The rheological analogue is depicted in Fig. 1. The rheological characteristic of the polymer and the interactions between the polymer and the filler determine the properties of the compound. Rheological oscillation experiments determine the whole spectrum of the viscoelastic properties in the frequency range. The complex viscosity **h*** or the complex shear modulus G^* describe the viscoelastic properties, as given in eq. 1.

$$|\eta^*| = |G^*| = G' + j\omega G'' \tag{1}$$

where G' is the storage modulus and represents the sum of the springs G_1 and G_2 in Fig. 1. The loss modulus G'' represents the dissipated energy as the sum of friction loss and plastic deformation. The dashpots η_0 and η_2 symbolize their contribution to the deformation γ.

B. Oscillation Measurements

Measurements were carried out by the use of an oscillation rheometer at controlled shear stress (CSR), which allows the diminution of the yield point [11]. Samples with a size of 10×30 mm^2 and a thickness of 1 mm were prepared. For this

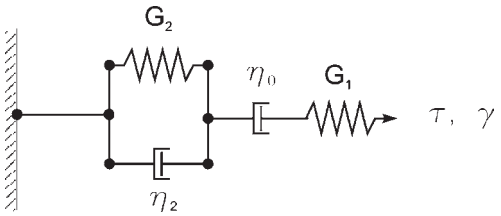

Fig. 1. Burgers model for viscoelastic solids [10].

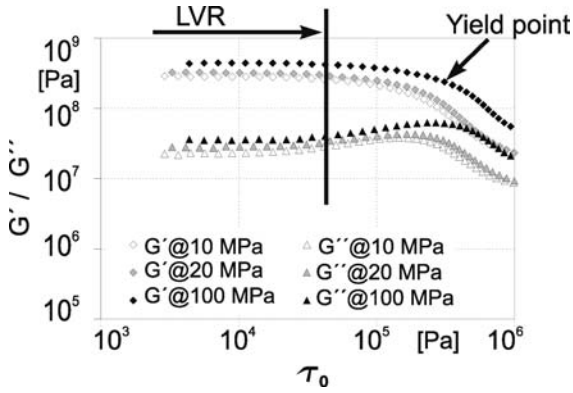

Fig. 2. Amplitude sweep at 60°C for samples with different compression.

purpose, four layers of the 951 AX tape were dried at 80°C for 10 min and laminated at 70°C for 5 min. The lamination pressure was varied. Samples were prepared at lamination pressures of 10 MPa, 20 MPa, and 100 MPa, to investigate the influence of the compression on the yield point. Fig. 2 depicts the obtained curves.

The linear viscoelastic range (LVR) specifies the load range in which no plastic deformation occurs. Above the limit strength of the LVR, crack formation starts. Within this range, storage and the lost modulus are not influenced by the load. Outside the LVR, the storage modulus begins to fall and the loss modulus increases due to the higher plastic deformation. The yield point is indicated by the breakdown of the storage modulus, which results from the collapse of the bonds between binder and filler. The average yield strength at 60°C for the standard lamination pressure of 20 MPa amounts to 186 kPa. It can be noted that an increase of the lamination pressure from 10 MPa to 100 MPa results in an approximate doubling of the yield strength from 1.2×10^5 Pa to 2.2×10^5 Pa. Stronger compression leads to tougher behavior, distinguishable by a moderate drop of the curves. Furthermore, the influence of the temperature on the yield point was investigated and the measured curves are depicted in Fig. 3.

It was found that the viscoelastic modulus and yield strength do not change significantly. The yield strain increases from 1.3% at 60°C to 1.6% at 100°C, indicating that the malleability of the binder increases. The material shows more brittle behavior at higher temperatures. This can be seen from a stronger curve drop beyond the yield point.

A temperature sweep was carried out at a constant deformation of 0.005% and an angular frequency of 10 s^{-1} to study the course of the viscoelastic modulus within the LVR. In this range G'' represents only the friction loss, because no plastic deformation occurs. Fig. 4 depicts the measurement results.

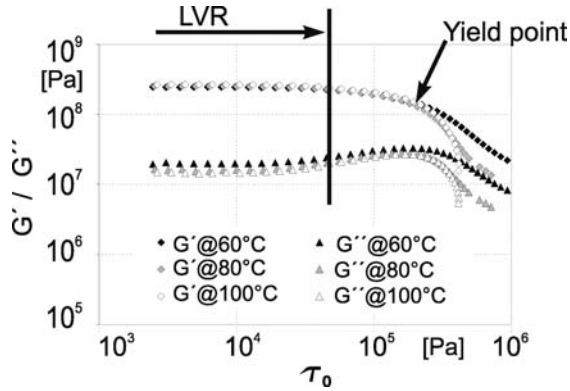

Fig. 3. Amplitude sweep curves for 951 at different temperatures.

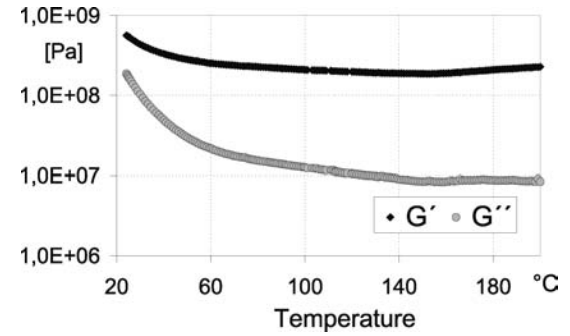

Fig. 4. Temperature sweep within the LVR at 10 s^{-1} and a deformation of 0.005%.

The storage modulus G' and the loss modulus G'' increase chiefly below a temperature of 60°C. No typical softening point is visible. Interactions between binder and filler dominate the viscoelastic behavior. Friction losses decrease with an increase of the temperature.

C. Creep Behavior

Creep recovery curves were measured with the purpose of investigating the relaxation of the 951 tape. Samples were prepared as described above in section B at a lamination pressure of 20 MPa. Different shear stresses, corresponding to a multiple of the yield point obtained from the amplitude sweep, were applied at a constant temperature of 60°. The zero-shear viscosity η_0 was calculated by means of the measuring software. The measured curves at different shear stresses are depicted in Fig. 5.

The retard time increases with the strength, the steady shear range is reached after 300 s for all curves. Elastic and plastic deformations are strongly influenced by the shear stress. If the shear strength increases from 279 kPa to 833 kPa, the zero-shear viscosity η_0 decreases from 1.8×10^{11} Pa·s to 7×10^9 Pa·s, the plastic deformation increases by one order from 0.004–0.04 and the elastic deformation increases to approximately eight times the amount, to 0.026.

Creep recovery curves, measured at a constant shear strength of 279 kPa (amounts to 1.5 times the yield strength) and temperatures of 60°C and 100°C, are depicted in Fig. 6.

The zero-shear viscosity decreases from 1.8×10^{11} Pa·s at 60°C to 7.0×10^{10} Pa·s at 100°C and the elastic deformation

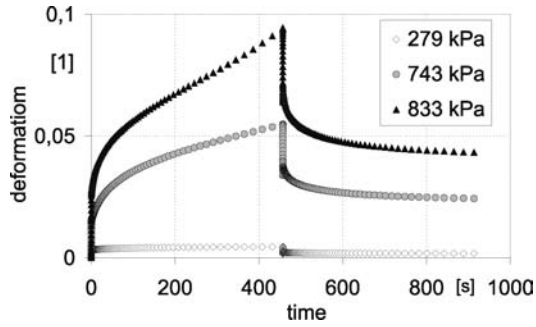

Fig. 5. Creep and creep recovery curve of 951, measured at 60°C at different shear strength.

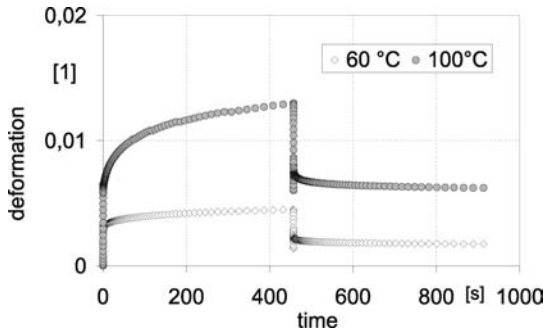

Fig. 6. Creep and creep recovery curve of 951, measured at different temperatures for a strain of 279 kPa.

doubles from 0.003–0.006. It can be noted that a change in the load has a stronger influence than a change in the temperature.

Characterization of the Embossing Process

A. Experimental Procedure

The main parameters for the embossing process are the temperature, the embossing pressure, the dwell time, and the friction coefficient of the arrangement. Among these parameters, no interactions are expected. Therefore, and with the intention to minimize the number of experiments, a matrix experiment (after Taguchi) was chosen. The results were analyzed by the use of a macro [12]. An overview of the parameters and their graduation is given in Table I. A reasonable temperature interval can be deviated from the temperature sweep in Fig. 4. The main drop of both viscoelastic moduli occurs below 60°C, and above 100°C there is no significant modification. Therefore, the temperature range was selected between these values. As the tapes are designed to adhere at the lamination temperature of 70°C, it has to be expected that adhesion also occurs between the tape and the tool and aggravates the demolding. The second process variable is the pressure. Yield points were determined for shear load. In the case of compressive load, the friction increases, therefore the applied load has to be increased. Earlier investigations have shown that the pressure should have values between 90 MPa and 120 MPa for good molding [5].

The creep recovery measurements depicted in Fig. 5 show that retardation processes fade after 300 s for all measurements. Therefore, the dwell time should be 5 min at least.

Table I
Process Variables and Their Graduations for the Matrix Experiment

	Graduation			
Variable	1	2	3	Unit
Pressure	90	105	120	MPa
Dwell time	5	10	15	min
Temperature	60	80	100	°C
Lubrication	none	oil	FC	—

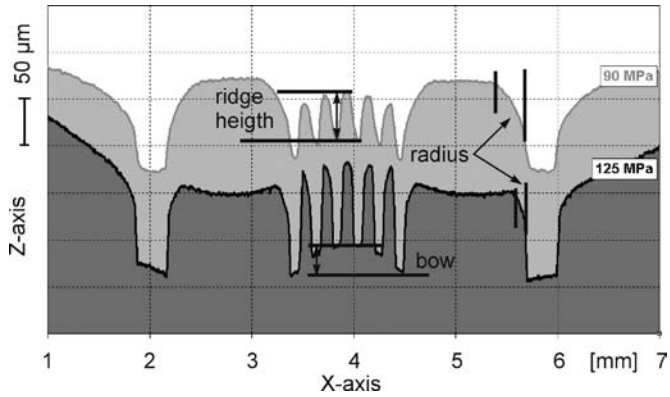

Fig. 7. Geometrical selection criteria for the experimental setup.

The maximum time was chosen as 15 min to limit the process time to a practicable value. The friction conditions were modified by the use of organic oil and flour carbon layers (FC), deposited by chemical vapor deposition with a thickness of 40 nm on the silicon tool. It is necessary to ensure that residues do not influence the lamination step that follows. For this reason, a test was carried out beforehand to rule out the possibility. Neither tapes treated with linseed oil nor ones treated with FC coated silicon tools showed delaminations.

Four selection criteria were chosen to evaluate the process conditions. The first criterion is the molding of fine ridges. It limits the structure distance and the depth of the embossed geometry. The ridge height h_r was measured for 50 µm wide patterns. The second criterion is the radius, which is formed on embossed edges, and the third is the bow, which occurs on large embossed structures. The geometric criteria are explained in Fig. 7.

The radius and bow were determined by means of an approximation of the profile scan data by a circle and the interpreted parameter was the respective radius. As a further criterion, the demolding behavior was assessed in accordance with the schema given in Table II. Marks 4 and 5 classify unacceptable demolding circumstances.

To reach more statistical reliability, each experiment was carried out twice. The factor trends, calculated from the analysis of means (ANOM), are depicted in Fig. 8 for all four selection criteria.

The analysis of variances (ANOVA) was carried out in accordance with Ref. [12]. The method compares the error variance of each experiment with the variances of the factor combinations in relation to the variability of the whole

process. Based on a reduction of variances, called the Fisher's method, conclusions were made on the significance of the respective factor on the process target. The comparison of the calculated values with an evaluation table (called Fisher's table) assess the factor's significance on the respective criterion. The results are summarized in Table III.

B. Discussion of the Results

The ANOM in Fig. 8a achieves the result that the best ridge forming occurs at the highest embossing pressure and at a temperature of 80°C or above with an oil-lubricated mold. The maximum value at the second graduation of the dwell time is made plausible by a stronger influence of other parameters within this experiment; the pressure and the surface state. The ANOVA clarifies that pressure and friction have significant influence, while dwell time and temperature are less important. The reason for this behavior is the dominance of the contact surface properties over the volume effects.

The best edge forming, characterized by a small radius, is achieved at maximum temperature and pressure. This follows from the ANOM in Fig. 8b. The drop of both viscoelastic moduli at higher temperatures, depicted in Fig. 4, leads to a better filling of cavities. From the ANOVA it follows that only the dwell time has no determinant influence on the criterion. The ANOM results for the bow are depicted in Fig. 8c. A high mean variation is noticeable. The ANOVA clarifies that no factor has a significant influence. Therefore other influences have to be considered in order to understand the phenomenon. A strong dependency is expected from the stress state, which is nominally defined by layout parameters. The best demolding conditions are achieved by the use of oil at a temperature of 60°C, see Fig. 8d. Fluor-carbon layers on the silicon mold do not improve the demolding. Temperatures of 80°C and above as well as dwell times above 10 min encourage adhesion. The ANOVA leads to the result that the surface conditions and the temperature have a strong influence, while pressure and dwell time are subordinate in importance.

It can be concluded that the friction strongly influences all regarded criteria, except the bow. Therefore, the surface state of the tool and the preparation of the tapes should be in the

Table II
Assessment Table for the Demolding Evaluation

Mark	Characteristic
1	Removed without external force
2	Demolding with light external force
3	Demolding with strong external force
4	Damage of single patterns
5	Tear of the whole tape

Table III
Summary of the Factor Significance, Extracted from the analysis of Variances

	h_{ridge}	Bow	Radius	Demolding
Pressure	Significant	No	High	No
Dwell time	No	No	No	No
Temperature	No	No	High	Significant
Lubrication	High	No	Significant	High

Significant = significant (95% threshold of Fisher's table)
High = highly significant (99% threshold of Fisher's table)
No = not significant

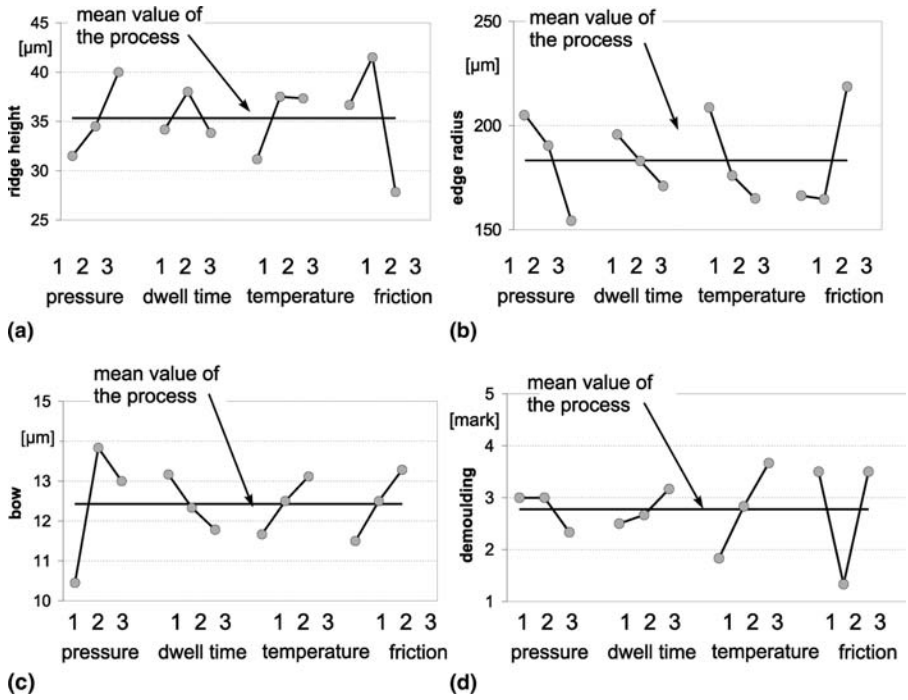

Fig. 8. Factor influence on all investigated criteria (ANOM) according to Ref. [12].

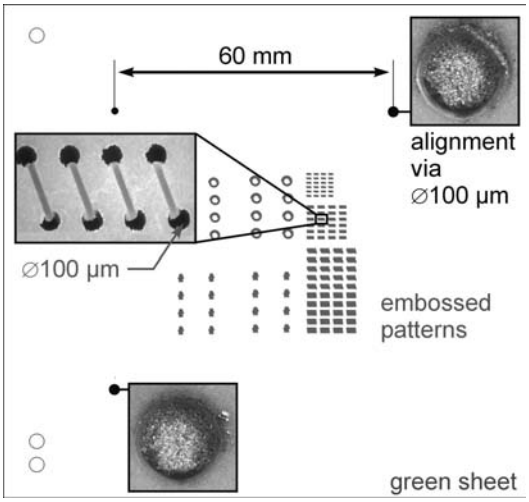

Fig. 9. Alignment of embossed patterns on a sheet with already punched vias (Ø100 µm).

focus of the process control. Higher temperature has a positive influence on the molding of edges, but the demolding aggravates. The dwell time has no significant influence on all investigated evaluation criteria. This is plausible, because the retardation time for all embossing conditions is less than the minimum dwell time of 5 min (compare Figs. 5 and 6). The pressure mainly influences the edge forming and the forming of fine patterns.

C. Position Tolerances of Embossed Patterns

A main requirement to ensure a stable process is the position constancy of embossed patterns. Long-time relaxation must be excluded to achieve practicable results. Under this aspect, the positions of embossed patterns were measured for five samples and compared with the design data. The layout is depicted in Fig. 9. Each measurement was carried out three times by means of a measuring microscope and the standard deviation of the method was determined. The dimension deviation from the design data were better than 30 µm referring to a length of 60 mm.

This value corresponds to the obtained standard deviation for the measurement. Afterward tapes were stored under constant humidity for one week and the measurements were repeated. A change of the results could not be observed, and the deviation of the second measurement was better than the first one. Patterns also were embossed into tapes with prepared vias and the position was hit with high accuracy, as shown in Fig. 9.

This establishes that the position tolerances are determined by the precision of the embossing tool.

Embossing of Sealing Elements

Integrated valves are basic components for dosage processes in complex fluid handling systems. Sealing patterns enhance the functionality of valve seats. The sealing depends on the surface quality, which is defined by evenness and roughness. Leak losses are generated by parasitic microchannels in the sealing set. An enlarged ductility of the sealing material,

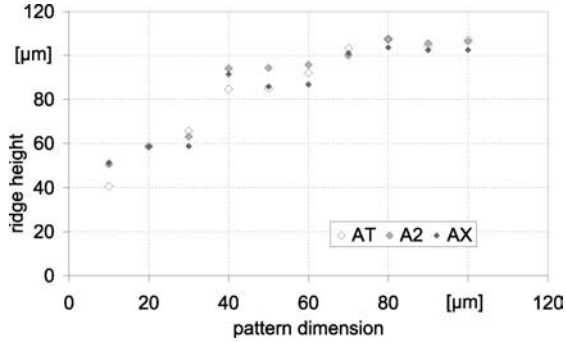

Fig. 10. Formation of small ridges without lubrication for different thicknesses of 951.

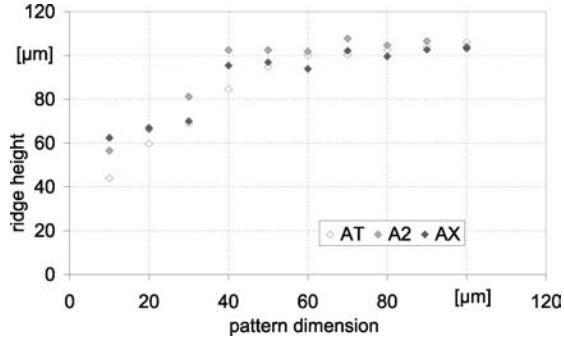

Fig. 11. Formation of small ridges under use of linseed oil as lubricant.

which is deformed because of the contact pressure, reduces the leakage cross section. Therefore three objectives have to be pursued to create a good seal: an even and smooth surface of the sealing seat, small sealing patterns to increase the contact pressure, and the use of a ductile material at the facing. If screen printed layers are fitted into a valve assembly, the ductility of the metal increases the sealing. It is expected that the roughness can be diminished by embossing and that the generation of fine seal lips reduces the leak loss.

A. Forming of Fine Patterns

In the previous section, the influence of the friction at the side walls of the mold was identified as the strongest on the formation of fine ridges. The quantitative dependency of pattern size and lubrication on the maximum height of embossed ridges was studied by the use of a test layout that contains lines and spaces from 10 µm to 100 µm width, and has a mold depth of 105 µm. A pressure of 100 MPa was applied at 55°C without and with lubricant. Single tape layers of the 951 tape system with different thickness were used. The tape is industrially available in thicknesses of 113 µm (AT), 165 µm (A2), and 254 µm (AX). The results are depicted in Figs. 10 and 11.

The smallest patterns with a line width of 10 µm form ridges with 50 µm height. For the thinnest tapes the ridge height is limited to 40 µm, indicating that the displaced material amount is too small to fill the hollows of the mold. The full mold depth is reached for pattern sizes of 70 µm and larger. Lubrication leads to better ridge formation, with 10 µm ridges reaching a height of approximately 60 µm, as shown in Fig. 11. In the AT tape, ridges with 44 µm height are formed. The total

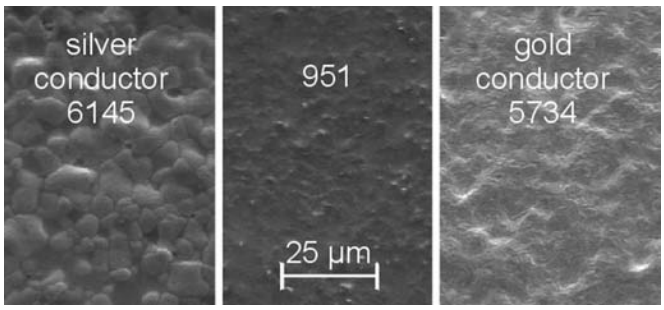

Fig. 12. Surface structure of sintered 951 and screen printed layers.

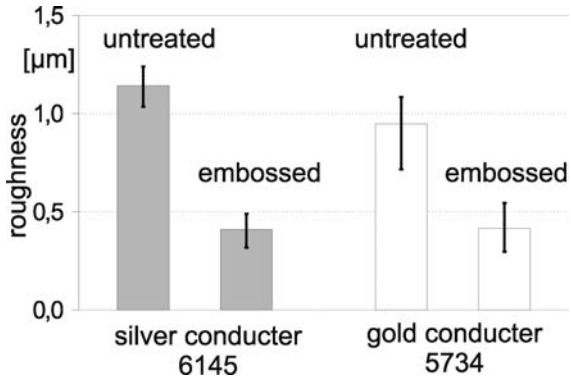

Fig. 13. Comparison of the roughness measured on untreated and embossed metallization layers.

depth of the mold is filled for structures of 50 µm and larger. Patterns embossed in AX tape result in smaller ridges than patterns in A2 tape as a consequence of tape elasticity. In general, friction conditions, the amount of displaceable material underneath the mold, and the elasticity of the tape limit the pattern size. Additionally, the stress causes distortion of thin tapes dependent on the embossed total area. Therefore, the depth of a mold should be limited depending on the thickness of the tape.

B. Smoothing of the Surface by Means of Embossing

Beyond the formation of small sealing rings, the reduction of the roughness is the second possibility to achieve better leakproof results. Therefore, the smoothing of fired 951 ceramic and compatible screen printed layers was investigated. Although embossing levels the surface of the green tape, the surface quality of the fired ceramic depends on the powder size of the LTCC tape and amounts to approximately 500 nm. Here it makes no difference whether the tape has been embossed or not. If printed layers are embossed, the ductility of the metal powders is presumed to cause a permanent smoothing. Therefore, the effect was studied for two different pastes, the silver conductor 6145 and the gold conductor 5437. Both were printed by means of an 80/40 polyester screen on 951 tapes. Average thicknesses of 17 µm for the silver conductor 6145 and 13 µm for the gold conductor 5734 were measured. Fig. 12 depicts SEM micrographs of the ceramic and the metallization surfaces after sintering.

Grain size and shape vary noticeably. The roughness of the untreated sintered metallization is larger than the roughness of the ceramic. To smooth the surface, the layers were embossed with a pressure of 100 MPa and the roughness was measured on the ridge, on the bottom, and on the untreated area after sintering. Molds that are 50 µm deep produced a smoothed surface only at the bottom of the patterns. If the depth of the mold is limited to 30 µm, smoothing is also achieved on the top of the ridges. In this way, useable sealing faces are fabricated. Fig. 13 depicts a diagram of the measured roughness on the top of a 30 µm high valve seat in comparison with the roughness of an untreated surface.

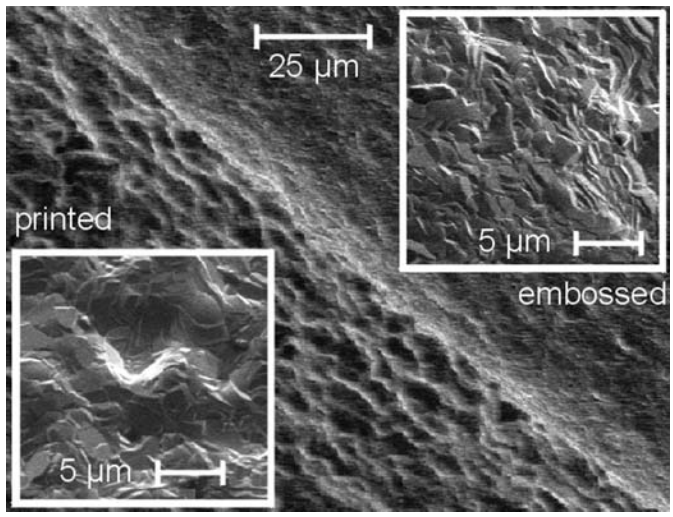

Fig. 14. SEM micrograph of the untreated and embossed surface of a gold metallization layer (paste 5734) after sintering.

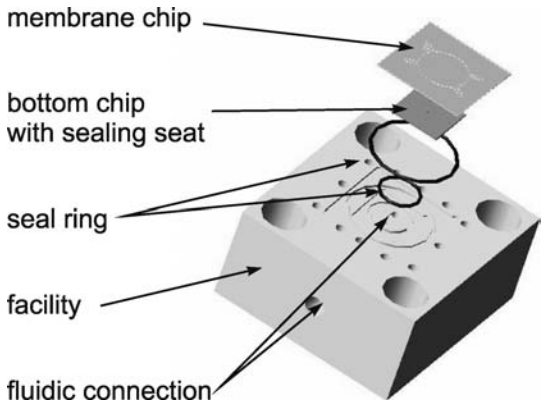

Fig. 15. Measurement assembly for leakage characterization.

For both metallization layers a roughness of 0.4 µm was achieved after sintering. This is better than the roughness of the pure ceramic, which amounts to 0.5 µm. Fig. 14 depicts SEM micrographs of embossed and printed surfaces. A clear smoothing can be seen.

Valve Seat Characterization

To quantify the sealing behavior of different facings, an experimental setup as shown in Fig. 15 was built up.

Two chips were prepared separately and fixed in the facility. The bottom chip includes prepared sealing patterns that

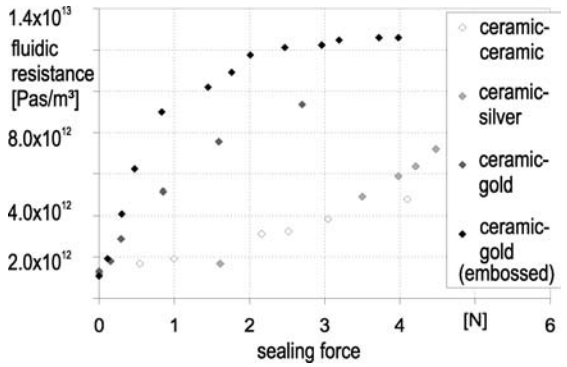

Fig. 16. Sealing force dependence of the fluidic resistance for different surface pairings.

consist of a plane ceramic surface, a printed ring of the silver conductor 6145 and of the gold conductor 5734, and an embossed sealing ring with a height of 30 μm into a 5734 layer. The membrane chip is built up by two layers of the 951 AT tape, the first one forms the membrane of 100 μm thickness and the second the fluid chamber, a cavity of 100 μm depth. The fluidic resistance of the assembly was determined as a function of the sealing force to evaluate the leakage behavior. For this purpose a constant flow of 0.05 mL/min was forced with high accuracy by an analysis pump and the pressure drop over the valve seat was measured. Fig. 16 depicts the measurement results.

The leakage characteristic of the ceramic-ceramic facing shows linear behavior. The reduction of the leak loss with increasing force is caused by coming closer to the surfaces; a deformation of the ceramic can be excluded. The silver conductor seal ring shows a different characteristic. As shown in Fig. 12, the fired layer consists of large particles that cause large leakage cross sections. With increasing sealing force, the cross section reduces due to the plastic deformation and the leakage characteristic can be approximated by a quadratic function. The smoother surface of the printed gold seat leads to a rapid rise of the leakage characteristic. The leakage behavior can be further improved by the use of an embossed sealing ring, the respective characteristic rises stronger than the printed sealing seat, caused by the smoothing of the sealing surface. In comparison with the ceramic facing, the leakage rate was improved by a factor of four at a force of 2 N.

A fully closed valve chamber was fabricated. The sealing patterns were embossed into one layer of the A2 tape. The bottom was reinforced by one AX tape and the membrane is formed by one layer of the AT tape. To prevent the collapse of the valve chamber during the lamination step, carbon paste was screen printed into the embossed cavity. The fitting-in of such pastes into the 951 multilayers is described in Hintz [13]. The whole stack was isostatically laminated at a pressure of 20 MPa and a temperature of 70°C and afterward sintered by the use of a standard process with an enhanced burnoff time. The chamber showed no cracks. To view the hollow, it was saw-cut. All carbon was completely evaporated. Fig. 17 depicts a cross section of the valve chamber.

The three-dimensional ring patterns are maintained during the process, and in the center of the embossed gold conductors

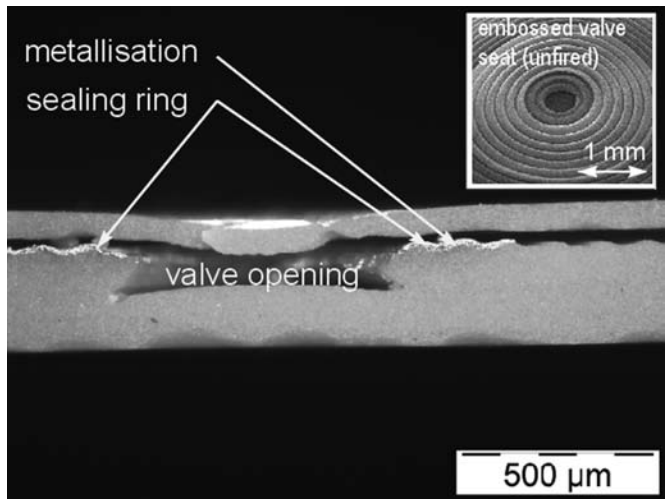

Fig. 17. Chamber and embossed sealing seat of a cofired valve assembly.

an elevated sealing ring is formed. Thus a ductile sealing element is generated inside of the fully ceramic fluid chamber.

Summary

The viscoelastic properties of Du Pont's 951 tapes were investigated. It was found that compression increases the toughness under shear stress. The main drop of both viscoelastic moduli were measured between room temperature and 60°C. The influences of the temperature, the pressure, the dwell time, and the friction on the embossing of single sheets were investigated under the use of design of experiments. As a result, the friction was identified as the strongest influence on the forming of the tapes. Dwell times longer than 5 min do not influence the embossing results significantly. The position tolerances of embossed patterns are determined from the position tolerance of the mold and no relaxation was observed over a period of one week. An aspect ratio for 30 μm wide lines and spaces of 2:1 was achieved. Smoothing of metallization layers by embossing is demonstrated. Sealing patterns made of screen printed layers and embossed sealing rings were characterized and the improvement of the leakage behavior was shown. In this way, the effectiveness of sealing patterns, manufactured under the exclusive use of thick film techniques, was proven. Embossed sealing elements were successfully integrated into a fully ceramic fluid chamber.

Acknowledgments

This work was funded by the Thuringian Ministry of Economics, Technology, and Labour within the project Kerafema. The authors thank all the members of the Center for Innovation Competence macronano for their kind collaboration and technical assistance.

References

[1] M.R. Gongora-Rubio, P. Espinoza-Vallejos, L. Sola-Laguna, and J.J. Santiago-Avilés, "Overview of low temperature cofired ceramic technology for meso-system technology," Sensors and Actuators A, Vol. 89, pp. 222-241, 2001.

[2] T. Thelemann, M. Fischer, A. Groß, and J. Müller, "LTCC based fluidic components for chemical applications," Journal of Microelectronics and Electronic Packaging, Vol. 4, No. 4, pp. 167-172, 2007.
[3] J. Park, P. Espinoza-Vallejos, L. Sola-Laguna, and J. Santiago-Aviles, "Etching and exfoliant techniques for the fabrication of 3-D meso-scales structures on LTCC tapes," MRS Fall Meeting 3582, pp. 121-126, 1998.
[4] Y.H. Park, C.R. Cho, I.T. Kim, M.W. Lee, K.T. Hwang, J.D. Yu, J.D. Mun, S.S. Kong, B.K. Kim, A.N. Sreeram, K. Palit, M. Liberatore, E. Tormey, L. Hozer, and A. Prabhu, "Fabrication of 165 μm pitched PDP back panel based on LTCC-M technology" in *2000 SID Digest*, pp. 478-481, 2000.
[5] A. Albrecht, J. Botiov, M. Fischer, K.-H. Drüe, M. Hintz, and H. Wurmus, "Alternative way to high current structures in LTCC," *Proceedings of the European Microelectronics Packaging Conference, Friedrichshafen,* 2003.
[6] L. Rebenklau, "*Beiträge zum Aufbau und zur Technologie LTCC-basierter mikrofluidischer Bauelemente und Systeme,*" Verlag Dr. Markus A. Detert, 1. Auflage, Templin, Germany, pp. 67-69, 2003.
[7] K. Vaed, J. Florkey, S.A. Akbar, M.J. Madou, J.J. Lannutti, and S.S. Cahill, "An additive micromolding approach for the development of micromachined ceramic subtrates for RF applications," Journal of Microelectromechanical Systems, Vol. 13, No. 3, pp. 514-525, 2004.
[8] T. Rabe, P. Kuchenbecker, and B. Schulz, "Hot embossing—An alternative method to produce cavities in ceramic multilayer," *Proceedings of the CICMT Conference,* 2006.
[9] H. Bartsch de Torres and M. Hoffmann, "Embossing of microfluidic structures in ceramic multilayers," *Proceedings of the Smart Systems Integration Conference,* Paris, March 27-28, 2007, pp. 423-426.
[10] P.J. Carreau, D.C.R. De Kee, and R.P. Chhabra, "*Rheology of Polymer Systems,*" Hanser/Gardner, Munich, chap. 5, p. 180, 1997.
[11] T. Mezger, "*Das Rheologie-Handbuch,*" Vincentz, Hannover, Germany, 2000.
[12] B. Klein, "*Versuchsplanung DoE,*" Oldenburg Wissenschaftsverlag GmbH, 2004.
[13] M. Hintz, "*Druckunterstütztes Sintern als Grundlage neuer Technologievarianten für LTCC,*" Verlag ISLE, 1. Auflage, Ilmenau, Germany, pp. 93-95, 2007.